Inorganic Chemistry

Article

pubs.acs.org/IC

Photoinduced Mixed Valency in Zinc Porphyrin Dimer of Triruthenium Cluster Dyads

Jane Henderson and Clifford P. Kubiak*

Department of Chemistry and Biochemistry, University of California—San Diego, 9500 Gilman Drive MC 0358, La Jolla, California 92093, United States

Supporting Information

ABSTRACT: The preparation, electrochemistry, and spectroscopic characterization of three new species, (ZnTPPpy)-$Ru_3O(OAc)_6(CO)$-pz-$Ru_3O(OAc)_6(CO)L$, where ZnTPPpy = zinc(II) 5-(4-pyridyl)-10,15,20-triphenylporphyin, L = pyridyl ligand, and pz = pyrazine, are reported. These porphyrin-coordinated Ru_3O–BL–Ru_3O (BL = bridging ligand) dyads are capable of undergoing intramolecular electron transfer from the photoexcited Zn porphyrin to Ru_3O donor–bridge–acceptor dimer systems. Seven reversible redox processes are observed in the cyclic voltammograms of the newly synthesized dyads, showing no significant electrochemical interaction between the redox active porphyrin and the pyrazine-bridged ruthenium dimer of Ru_3O trimers. From the electrochemical behavior of the dyads, large comproportionation constants ($K_c = 6.0 \times 10^7$ for L = dmap) were calculated from the reduction potentials of the $Ru^{III}Ru^{III}Ru^{II}$ clusters, indicating a stable mixed-valence state. Electronic absorption spectra of the singly reduced mixed-valence species show two intervalence charge transfer (IVCT) bands assigned within the Brunschwig–Creutz–Sutin semiclassical three-state model as metal-to-bridge and metal-to-metal in character. The progression from most to least delocalized mixed-valence dimer ions, as determined by the divergence of the IVCT bands and in agreement with electrochemical data, follows the order of L = 4-dimethylaminopyridine (dmap) > pyridine (py) > 4-cyanopyridine (cpy). These systems show dynamic coalescence of the infrared spectra in the ν(CO) region of the singly reduced state. This sets the time scale of electron exchange at <10 ps. The electron transfer from the S_1 excited state of the coordinated porphyrin to the dimer is predicted to be thermodynamically favorable, with ΔG^0_{FET} ranging from −0.54 eV for L = dmap to −0.62 eV for L = cpy. Observation of IVCT band growth under continual photolysis (λ_{exc} = 568 nm) confirms a phototriggered intramolecular electron transfer process resulting in a strongly coupled singly reduced mixed-valence species.

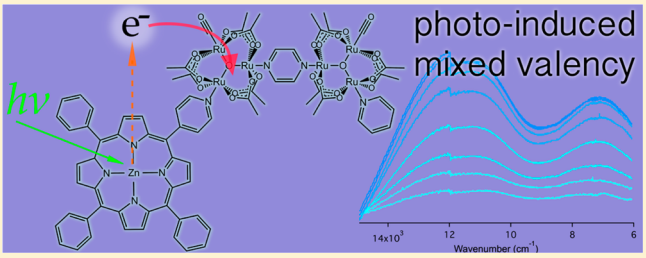

INTRODUCTION

In order to better understand photoinduced electron transfer and the charge-transport properties of molecules, donor–acceptor systems capable of generating an energy-rich and long-lived charge separation state upon illumination have been intensively studied.[1−12] The charge separation efficiency in species of this type can be predicted *a priori* through characterization of excited-state energies and electrochemical behavior in the ground state.[6,13−15] Long-lived charge-separated states can be stabilized through deliberate geometric modifications of the electronic coupling between the donor and acceptor, tuning the rates of forward and back electron transfer.[5,7,15−21] Apart from these synthetic modifications, other elements of electronic coupling are typically difficult to predict, and new molecular systems ususally build upon previously established trends in electronic coupling.[14,22−24] In order to study the broadly impacting dynamics of electron delocalization resulting from electron reduction, we designed a series of donor–bridge–acceptor molecules capable of undergoing a phototriggered intramolecular electron transfer process resulting in strongly electronically coupled mixed-valence systems. These systems have allowed us to generate a stable mixed-valence state, observable by intervalence charge-tranfer (IVCT) bands, following continual photolysis.

These systems are based on the tris-ruthenium oxo-centered cluster dimers introduced by Ito and co-workers in 1996, which upon a single electron reduction, form delocalized mixed-valence systems.[25−31] Electrochemical characterization of $[Ru_3(\mu_3\text{-}O)(\mu\text{-}CH_3CO_2)_6(CO)(L)]_2$-BL, where L = a pyridyl ligand and BL = pyrazine (pz), shows two sequential one-electron metal-based reductions. The splitting of these reduction waves (ΔE) can be used to determine the comproportionation constant (K_c) using the equilibrium equation for the comproportionation reaction of the singly reduced mixed-valence state. K_c is frequently used as a measure for the extent of electronic communication between the two redox-active centers of a given mixed-valence dimer and is on the order of 10^7 for L = 4-dimethylaminopyridine (dmap).[26] The electronic delocalization in these dimers has been further

Received: August 10, 2014
Published: September 26, 2014

dx.doi.org/10.1021/ic501889u | *Inorg. Chem.* 2014, 53, 11298−11306

characterized by the coalescence of the carbonyl ν(CO) band shapes in the 1D IR spectra of mixed-valence dimers, allowing for the observation of electron transfer dynamics on the vibrational time scale.[25,26,32−34] Application of the Brunschwig−Creutz−Sutin (BCS) semiclassical three-state (metal cluster−bridge−metal cluster) model of mixed valency accounts well for the appearance of two IVCT bands observed in the near-IR (NIR) region of the electronic absorption spectra of these mixed-valence ions.[29,35] In the most delocalized case, the intensity of the IVCT bands of the singly reduced mixed-valence state allows the electronic coupling across the system to be characterized as borderline Robin−Day class II/III, corresponding to L = dmap.[36] These dimers represent systems whose electronic coupling, evident in electronic delocalization, can be adjusted on the basis of the electronic properties of the ancillary ligands.

The molecular dynamics occurring as the singly reduced dimer of Ru_3O clusters evolves to the delocalized mixed-valence state is not fully understood, as reduction of the dimer to the state of interest has been limited to chemical or electrochemical means. Electron transfer dynamics occurring in these mixed-valence ions is predicted to be occurring on the picosecond time scale; therefore, the mixed-valence state has only ever been explored well after delocalization has been established.[34,37] In order to resolve the time scales of the dynamics occurring at the earliest stages of delocalization, ultrafast (<10 ps) measurement techniques are required.[38−40] These time scales require optical pump−probe spectroscopy, where the initial reduction can be photoinduced. To accomplish this, we have synthesized dyads **1**−**3** (Figure 1), allowing a light-induced reduction via an excited zinc(II) *meso*-5-(4-pyridyl)-10,15,20-triphenylporphyin coordinated to one of the Ru_3O clusters. Using the method of Lindsey and co-workers for asymmetric porphyrin design, the monopyridyl-functionalized porphyrin was synthesized and coordinated to one of the two ancillary (L) positions of the dimer.[31,41,42] The choice of ancillary ligand on the Ru_3O cluster opposite the porphyrin, L = dmap, pyridine (py), or 4-cyanopyridine (cpy), allows for variation in the electronic coupling in the mixed-valence ion. Through full characterization of the vibrational and electronic dynamics of neutral and singly reduced species, the systems display trends resulting from delocalization analogous to the symmetric pyridine derivatives but function as a photoresponsive homologue to our previously explored mixed-valence library.[32,33] The ability to generate the singly reduced species following light exposure was confirmed through continuous photolysis in the presence of a sacrificial donor. In this study we demonstrate the observation of strong electronic coupling resulting from photoreduction in donor−bridge−acceptor molecules and explore the possibility of electron and energy transfer in these systems.

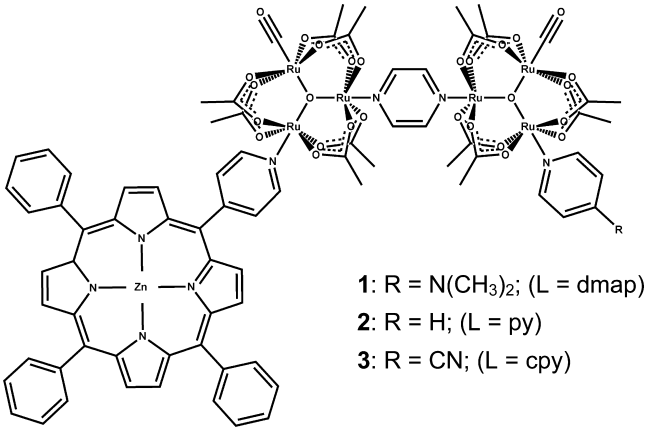

Figure 1. Newly synthesized asymmetric $[Ru_3(\mu_3\text{-}O)(\mu\text{-}CH_3CO_2)_6(CO)$(5-(4-pyridyl)-10,15,20-triphenylporphyinatozinc-(II))$](\mu\text{-}pz)[Ru_3(\mu_3\text{-}O)(\mu\text{-}CH_3CO_2)_6(CO)(L)]$ (**1**−**3**). Variations of the R group of the ancillary pyridine allow for tuning of the electronic communication across the molecule.

EXPERIMENTAL SECTION

General Methods. ^{1}H NMR spectra were recorded on a JEOL 500 MHz spectrometer. Elemental analysis was performed by Numega Resonance Laboratories, San Diego, CA. Automated column chromatography was carried out on a CombiFlash R_f200 (Teledyne Isco, 40 g silica column, 0−5% methanol in chloroform). All chemicals and solvents for synthesis were obtained from Fisher Scientific and used as received. Tetra-*n*-butylammonium hexafluorophosphate ($TBAPF_6$) was received from Sigma-Aldrich, recrystallized from absolute ethanol, and dried under vacuum at 100 °C for 24 h. Decamethylcobaltocene ($CoCp^*_2$) and decamethylferrocene ($FcCp^*_2$) were used as received from Sigma-Aldrich. Potassium graphite (KC_8) was prepared as previously reported.[43] Air-sensitive reactions were carried out under a N_2 inert atmosphere in distilled butyronitrile stored over 3 Å molecular sieves. 1-Benzyl-1,4-dihydronicotinamide (BNAH) was purchased from TCI and used as received.

Absorption and Emission Spectroscopy. UV−vis−NIR spectra were collected with a Shimadzu UV 3600, and IR spectra were collected on a Thermo Scientific Nicolet 6700 FTIR. Steady-state fluorescence emission spectra were measured on a PerkinElmer LS-45. During emission measurements the optical density was kept below 0.1 at the excitation wavelength. KC_8 and $CoCp^*_2$ were added stoichiometrically to generate the singly and doubly reduced species. Samples were contained in Specac sealed liquid IR cells with CaF_2 windows and a path length of 1.00 mm. Spectral deconvolution of NIR spectra was carried out in IGORpro.

Electrochemical Measurements. Cyclic voltammetry was preformed using a BASi Epsilon voltammetric analyzer with a scan rate of 100 mV/s. A 3 mm glassy carbon electrode was used as the working electrode. The counter electrode was a platinum wire, and the reference electrode was a Ag/AgCl wire. Electrochemical solutions were prepared as a 3 mM solution of complex in 0.1 M $TBAPF_6$ butyronitrile electrolyte solution degassed with N_2. $FcCp^*_2$ was used as an internal reference for each sample ($FcCp^*_2{}^{+/0}$ = −0.125 V vs SCE in acetonitrile).[44]

Preparation of Porphyrin Coordinated, Pyrazine-Bridged Dyads. The synthesis of $[Ru_3(\mu_3\text{-}O)(\mu\text{-}CH_3CO_2)_6(CO)(py)]_2(\mu\text{-}pz)$ ($\mathbf{2}_{sym}$), 5-(4-pyridyl)-10,15,20-triphenylporphyin (TPPpy), and zinc-(II) 5-(4-pyridyl)-10,15,20-triphenylporphyin (ZnTPPpy) have been reported previously.[25,26,41,42,45] The free-base asymmetric porphyrin was attached to the $Ru_3O(CH_3CO_2)_6(CO)(S)_2$ (where S = solvent) cluster, the synthesis of which has also been previously described.[31] Zinc insertion was achieved following porphyrin coordination to the ruthenium cluster.[46] The asymmetric dyads were synthesized by reacting equimolar quantities of the monoporphyrin-substituted cluster $Ru_3O(CH_3CO_2)_6(CO)$(ZnTPPpy)(S) (**ii**) and Ru_3O-$(CH_3CO_2)_6(CO)(L)$(pz) (where L = dmap, py, or cpy), the syntheses of which have been previously described.[25,26]

$Ru_3(\mu_3\text{-}O)(\mu\text{-}CH_3CO_2)_6(CO)$(TPPpy)(S) (i). A reaction mixture of 0.8 equiv of TPPpy (147 mg, 0.22 mmol) dissolved in 50 mL of chloroform slowly added to 1 equiv of $Ru_3O(\mu_3\text{-}O)(\mu$-$CH_3CO_2)_6(CO)(S)_2$ (200 mg, 0.27 mmol) in 50 mL methanol was stirred at room temperature for 2 days in the dark. The solution was evaporated to dryness and the monosubstituted product was purified on an automated column chromatograph. Typical yield 60%. Anal. Calcd for $C_{56}H_{47}N_5O_{14}Ru_3 \cdot {}^3/_2CH_2Cl_2$: C 47.81; H, 3.49; N, 4.85.

dx.doi.org/10.1021/ic501889u | *Inorg. Chem.* 2014, 53, 11298−11306

Scheme 1. Nomenclature and Synthetic Scheme[a]

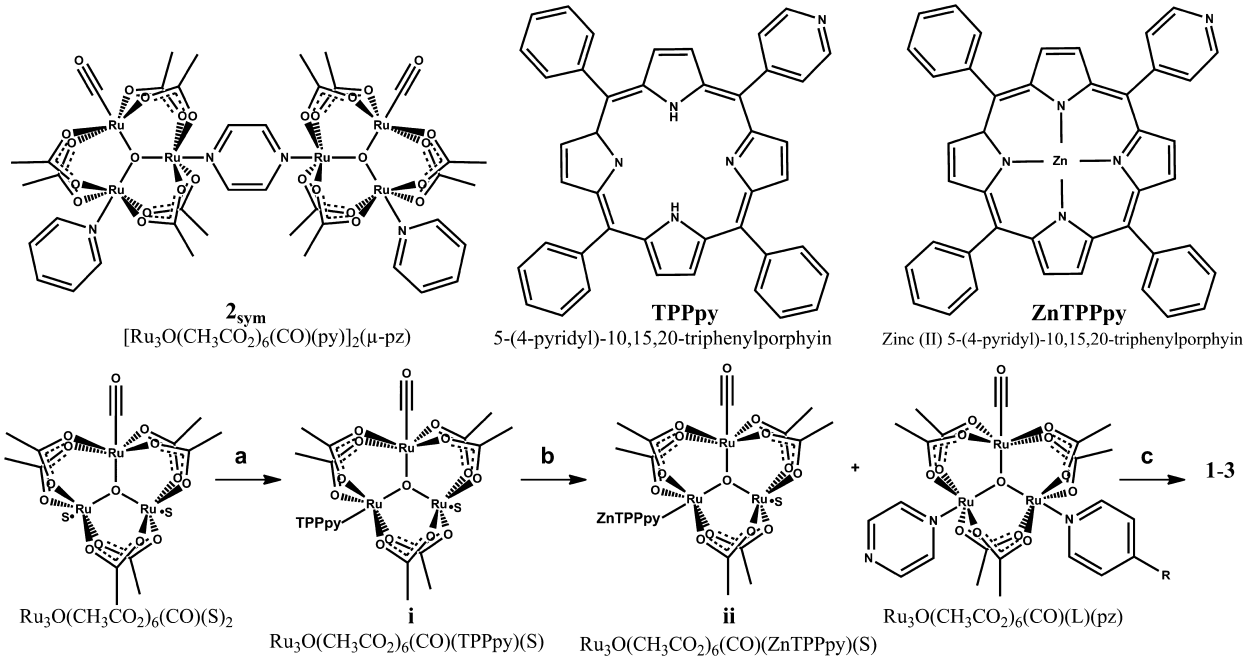

[a]Reagents and conditions: (a) 0.8 equiv of TPPpy/1 equiv of $Ru_3(\mu_3\text{-}O)(\mu\text{-}CH_3CO_2)_6(CO)(S)_2$ stirred in chloroform/methanol at room temperature for 2 days in the dark. Complex **i** was purified on an automated column chromatograph. (b) 2 equiv of zinc acetate methanol solution refluxed for 30 min in 1 equiv of **i** in chloroform, followed by chromatography on silica treated with 5% TEA. (c) Equimolar amounts of **ii** and $Ru_3(\mu_3\text{-}O)(\mu\text{-}CH_3CO_2)_6(CO)(L)(pz)$ allowed to react in the dark for 2 days at rt.

Found: C, 47.48; H, 3.96; N, 5.24. ^{1}H NMR (500 MHz, $CDCl_3$) δ: 9.67 (d, J = 5.9 Hz, 2H, 2,6-pyridyl), 9.31 (d, J = 4.5 Hz, 2H, β-pyrrole), 9.03 (d, J = 4.5 Hz, 2H, β-pyrrole), 8.95 (d, J = 5.9 Hz, 2H, 3,5-pyridyl), 8.90 (s, 4H, β-pyrrole), 8.24 (d, J = 6.9 Hz, 6H, o-phenyl), 7.83−7.74 (m, 9H, m- and p-phenyl), 2.33 (s, 6H, acetates CH_3), 2.25 (s, 6H, acetates CH_3), 2.09 (s, 6H, acetates CH_3), −2.69 (s, 2H, internal pyrrole). IR (butyronitrile): ν(CO) 1939 cm^{-1}. UV−vis (butyronitrile): λ_{max}/nm = 417, 514, 551, 590, 647.

$Ru_3(\mu_3\text{-}O)(\mu\text{-}CH_3CO_2)_6(CO)(ZnTPPpy)(S)$ (ii). A solution of **i** (100 mg, 0.075 mmol) dissolved in 50 mL of chloroform was added to 2 equiv of zinc acetate (33 mg, 0.15 mmol) dissolved in <5 mL of methanol. This mixture was heated at reflux for 30 min, allowed to cool, and dried. Full zinc insertion was determined by NMR prior to further purification. The product was purified using automated column chromatography on silica treated with 5% TEA. Typical yield 80%. Anal. Calcd for $C_{56}H_{45}N_5O_{14}Ru_3Zn{\cdot}CH_2Cl_2{\cdot}2CH_3OH$: C, 46.33; H, 3.62; N, 4.58. Found: C, 46.01; H, 3.91; N, 4.72. ^{1}H NMR (500 MHz, $CDCl_3$) δ: 9.67 (d, J = 5.8 Hz, 2H, 2,6-pyridyl), 9.39 (d, J = 4.6 Hz, 2H, β-pyrrole), 9.11 (d, J = 4.6 Hz, 2H, β-pyrrole), 9.00−8.93 (m, 6H, β-pyrrole, 3,5-pyridyl), 8.23−8.21 (m, 6H, o-phenyl), 7.78−7.73 (m, 9H, m- and p-phenyl), 2.31 (s, 6H, acetates CH_3), 2.20 (s, 6H, acetates CH_3), 2.03 (s, 6H, acetates CH_3). IR (butyronitrile): ν(CO) 1939 cm^{-1}. UV−vis (butyronitrile): λ_{max}/nm = 425, 558, 602.

$[Ru_3(\mu_3\text{-}O)(\mu\text{-}CH_3CO_2)_6(CO)(ZnTPPpy)](\mu\text{-}pz)[Ru_3(\mu_3\text{-}O)(\mu\text{-}CH_3CO_2)_6(CO)(dmap)]$ (1). Equimolar amounts of **ii** (75 mg, 0.054 mmol) and $Ru_3(\mu_3\text{-}O)(\mu\text{-}CH_3CO_2)_6(CO)(dmap)(pz)$ (48 mg, 0.054 mmol) were allowed to react in the dark for 2 days at room temperature. The solution was evaporated to dryness and filtered, and the porphyrin-coordinated dyad was separated from the monomer by gel filtration (Bio-Beads SX-1 in $CHCl_3$). Typical yield: 20%. Anal. Calcd for $Ru_6C_{80}H_{77}N_9O_{28}Zn$: C, 42.06; H, 3.40; N, 5.52. Found: C, 42.04; H, 3.37; N, 5.62. ^{1}H NMR (500 MHz, $CDCl_3$) δ: 9.48 (d, J = 6.3 Hz, 2H, 2,6-pyridyl), 9.40 (d, J = 4.6 Hz, 2H, β-pyrrole), 9.35 (d, J = 3.6 Hz, 2H, pz), 9.29 (d, J = 3.6 Hz, 2H, pz), 9.13 (d, J = 4.6 Hz, 2H, β-pyrrole), 9.00 (s, 4H, β-pyrrole), 8.98−8.92 (m, 4H, 3,5-pyridyl, 2,6-dmap), 8.27−8.24 (6H, m, o-phenyl), 7.82−7.76 (m, 9H, m- and p-phenyl), 7.24 (d, J = 7 Hz, 2H, 3,5-dmap), 3.34 (s, 6H, dmap methyl) 2.33 (s, 6H, acetates CH_3), 2.32 (s, 6H, acetates CH_3), 2.23 (s, 6H, acetates CH_3), 2.16 (s, 6H, acetates CH_3), 2.11 (s, 6H, acetates CH_3), 1.97 (s, 6H, acetates CH_3). IR (butyronitrile): ν(CO) 1939 cm^{-1}. UV−vis (butyronitrile): λ_{max}/nm ($\varepsilon \times 10^3$ M^{-1} cm^{-1}) = 424 (530), 558 (41), 604 (32).

$[Ru_3(\mu_3\text{-}O)(\mu\text{-}CH_3CO_2)_6(CO)(ZnTPPpy)](\mu\text{-}pz)[Ru_3(\mu_3\text{-}O)(\mu\text{-}CH_3CO_2)_6(CO)(py)]$ (2). The same procedure for making **1** was employed for making **2** using $Ru_3(\mu_3\text{-}O)(\mu\text{-}CH_3CO_2)_6(CO)(py)(pz)$ (46 mg, 0.054 mmol). Typical yield: 15%. Anal. Calcd for $Ru_6C_{78}H_{72}N_8O_{28}Zn$: C, 41.80; H, 3.24; N, 5.00. Found: C, 41.85; H, 3.60; N, 4.80. ^{1}H NMR (500 MHz, $CDCl_3$) δ: 9.47 (d, J = 6.0 Hz, 2H, 2,6-pyridyl), 9.40 (d, J = 4.8 Hz, 2H, β-pyrrole), 9.23 (s, 4H, pz), 9.13 (d, J = 4.8 Hz, 2H, β-pyrrole), 9.01 (s, 4H, β-pyrrole), 8.99−8.93 (m, 4H, 3,5-pyridyl, 2,6-py), 8.27−8.16 (m, 7H, o-phenyl and 4-py), 8.06 (m, 2H, 3,5-py), 7.81−7.77 (m, 9H, m- and p-phenyl), 2.32 (s, 6H, acetates CH_3), 2.31 (s, 6H, acetates CH_3), 2.27 (s, 6H, acetates CH_3), 2.16 (s, 12H, acetates CH_3), 2.02 (s, 6H acetates CH_3). IR (butyronitrile): ν(CO) 1939 cm^{-1}. UV−vis (butyronitrile): λ_{max}/nm ($\varepsilon \times 10^3$ M^{-1} cm^{-1}) = 428 (470), 562 (30), 606 (21).

$[Ru_3(\mu_3\text{-}O)(\mu\text{-}CH_3CO_2)_6(CO)(ZnTPPpy)](\mu\text{-}pz)[Ru_3(\mu_3\text{-}O)(\mu\text{-}CH_3CO_2)_6(CO)(cpy)]$ (3). The same procedure for making **1** was employed for making **3** using $Ru_3(\mu_3\text{-}O)(\mu\text{-}CH_3CO_2)_6(CO)(cpy)(pz)$ (47 mg, 0.054 mmol). Typical yield: 10%. Anal. Calcd for $Ru_6C_{79}H_{71}N_9O_{28}Zn{\cdot}CHCl_3$: C, 40.28; H, 3.04; N, 5.28. Found: C, 40.43; H, 3.05; N 5.54. ^{1}H NMR (500 MHz, $CDCl_3$) δ: 9.45 (d, J = 5.6 Hz, 2H, 2,6-pyridyl), 9.39 (d, J = 4.7 Hz, 2H, β-pyrrole), 9.29 (d, J = 4.2 Hz, 2H, pz), 9.15−9.12 (m, 4H, β-pyrrole and pz), 8.98 (s, 4H, β-pyrrole), 8.93 (d, J = 6.5 Hz, 2H, 3,5-pyridyl), 8.76 (d, J = 6.7 Hz, 2H, 2,6-cpy), 8.27−8.23 (m, 8H, o-phenyl and 3,5-cpy), 7.81−7.77 (m, J = 6.2 Hz, 9H, m- and p-phenyl), 2.32 (s, 6H, acetates CH_3), 2.31 (s, 6H, acetates CH_3), 2.27 (s, 6H, acetates CH_3), 2.18 (s, 6H, acetates CH_3), 2.16 (s, 6H, acetates CH_3), 2.05 (s, 6H, acetates CH_3). IR (butyronitrile): ν(CO) 1941 cm^{-1}. UV−vis (butyronitrile): λ_{max}/nm (ε x10^3 M^{-1} cm^{-1}) = 425 (430), 560 (31), 605 (25).

Continuous Photolysis. Samples were prepared under a N_2 atmosphere. A 1 × 1 cm^2 quartz cuvette (Spectrocell, P/N RF-4010-T) containing a micostirbar (Starna, P/N MSB-6 × 1.5) was prepared carefully to prevent light exposure prior to photolysis. A 2

dx.doi.org/10.1021/ic501889u | Inorg. Chem. 2014, 53, 11298−11306

mL solution of 50 μM complex in butyronitrile was filtered directly into the cuvette. Then 250 μL of a filtered solution of 5 mM BNAH and 1 M $TBAPF_6$ in butyronitrile was added and the cuvette was quickly sealed. Photolysis was performed using the 568.2 nm line from a Coherent Innova 70C Ar^+/Kr^+ laser. The 65 mW beam was defocused to fully illuminate the 5 × 1 cm^2 cross-sectional area of the cuvette. Samples were irradiated for 50 min with constant stirring.

RESULTS AND DISCUSSION

Synthesis of $[Ru_3(\mu_3\text{-}O)(\mu\text{-}CH_3CO_2)_6(CO)(ZnTPPpy)](\mu\text{-}pz)[Ru_3(\mu_3\text{-}O)(\mu\text{-}CH_3CO_2)_6(CO)(L)]$ (1−3). The syntheses of $[Ru_3(\mu_3\text{-}O)(\mu\text{-}CH_3CO_2)_6(CO)(py)]_2(\mu\text{-}pz)$ ($\mathbf{2}_{sym}$), TPPpy, and ZnTPPpy have been reported previously.[25,26,41,42,45] The monosolvento complex $Ru_3(\mu_3\text{-}O)(\mu\text{-}CH_3CO_2)_6(CO)(TPPpy)(S)$ (**i**) was prepared similarly to other pyridine derivatives, by reacting $Ru_3O(\mu_3\text{-}O)(\mu\text{-}CH_3CO_2)_6(CO)(S)_2$ with 0.8 equiv of the free-base porphyrin TPPpy (Scheme 1). The desired monosubstituted cluster was purified from the doubly substituted cluster using column chromatography.[31] Metalation of the coordinated porphyrin was achieved via 30 min reflux of **i** in chloroform with 2 equiv of zinc acetate added as a methanol solution. Reaction completion was confirmed by the absence of the high-field ^1H NMR resonance from the inner pyrrole. This reaction mixture was purified using column chromatography on silica treated with 5% TEA to afford $Ru_3(\mu_3\text{-}O)(\mu\text{-}CH_3CO_2)_6(CO)(ZnTPPpy)(S)$ (**ii**) in good yield (80%).[46]

The dyads **1**−**3** (Figure 1), which have one carbonyl per Ru_3O unit and asymmetric pyridyl coordination, were prepared by a combination synthetic strategy using a labile ligand solvento species (**ii**) and $Ru_3(\mu_3\text{-}O)(\mu\text{-}CH_3CO_2)_6(CO)(L)(pz)$ (where L = dmap, py, or cpy) metal complex as the ligand.[47] The vacant Ru coordination site of **ii** allows for selective coordination to the free pyrazine nitrogen of the respective ancillary ligand monomer. The resulting porphyrin-coordinated assemblies (**1**−**3**) were isolated from their monomeric parts using size exclusion chromatography. In the neutral isolated state, each trinuclear Ru_3O unit formally contains one Ru(II) and two Ru(III) centers, with a carbonyl ligand coordinated to the formally divalent center.[29,34] This modular synthesis was used to generate the series of dyads **1**−**3**, which represent a continuum from electron withdrawing (L = cpy, **3**) to electron donating (L = dmap, **1**) substituents.

Steady-State Electronic Spectroscopy. Figure 2 shows the neutral, ground-state electronic absorption spectra of the symmetric py ancillary ligand pyrazine bridged dimer ($\mathbf{2}_{sym}$), ZnTPPpy, and **2** in butyronitrile. The absorption of the asymmetric porphyrin dyad strongly resembles that of ZnTPPpy, displaying an intense Soret band (λ_{max}/nm = 426 for ZnTPPpy and 428 for **2**) and two Q-bands [λ_{max}/nm Q(0−1)/Q(0−0) = 558/602 for ZnTPPpy and 562/606 for **2**]. The Soret of ZnTPPpy is less broad and more intense (ε = 550 × 10^3 M^{-1} cm^{-1}) in comparison to that of **2** (ε = 470 × 10^3 M^{-1} cm^{-1}). The strongly absorbing Q-bands of the porphyrin overlap with the broad metal-to-ligand charge-transfer (MLCT) transitions of the Ru_3O dimer, observed at 602 nm in $\mathbf{2}_{sym}$. Apart from a small red shift (ca. 0.01 eV) in peak absorbance energy observed in the asymmetric porphyrin/pyridine dyad (**2**), a ground-state electronic interaction between the Zn porphyrin and the Ru_3O dimer is not observed.

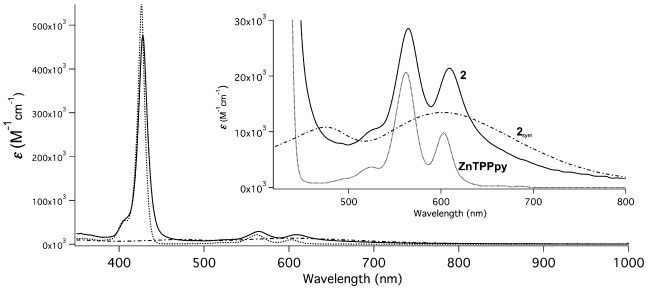

Figure 2. Electronic absorption spectra of the symmetric pyridine ancillary ligand pyrazine-bridged dimer ($\mathbf{2}_{sym}$), ZnTPPpy, and asymmetric porphyrin/pyridine dyad (**2**) in butyronitrile.

The steady-state fluorescence spectrum of ZnTPPpy in butyronitrile shows two bands centered at 610 and 658 nm, corresponding to the Q(0−0) and Q(1−0) emission transitions (Figure S1, Supporting Information). This fluorescence response is quenched upon coordination to the Ru_3O cluster, as shown by the fluorescence emission for **ii**. The lowest excited singlet-state energy (2.0 eV) of ZnTPPpy was determined from the average of the lowest energy transition in the absorption spectra and the highest energy transition in the fluorescence emission spectra.

Cyclic Voltammetry. The cyclic voltammograms (CVs) of **1**−**3** show seven reversible redox processes (Figures 3 and 4).

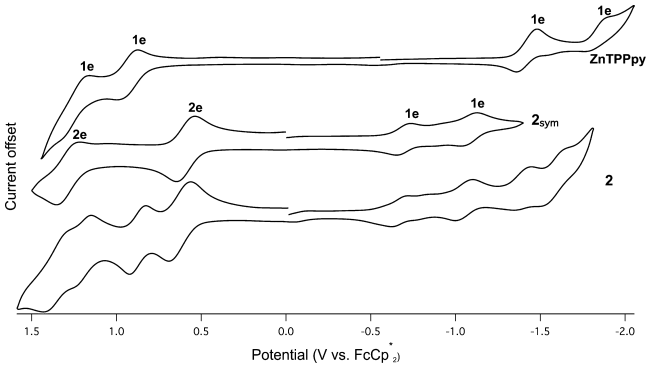

Figure 3. Cyclic voltamograms (scan rate of 100 mV/s) of ZnTPPpy (top), $\mathbf{2}_{sym}$ (middle), and **2** (bottom) with butyronitrile solvent and 0.1 M $TBAPF_6$ supporting electrolyte. Potentials are referenced to an external reference ($FcCp^*_2$).

To confidently assign each process, the CVs of ZnTPPpy, $\mathbf{2}_{sym}$, and **2** were compared to assign redox features characterized by the half-wave potentials for each process, $E_{1/2}$(ox/red) (Figure 3). The two-electron oxidation features observed in the porphyrin dyad (**2**) are Ru_3O metal-cluster based. Analogous redox features to these are observed in $\mathbf{2}_{sym}$ and occur at $E_{1/2}(+2/0)$ = +0.57 and $E_{1/2}(+4/+2)$ = +1.3 V vs $FcCp^*_2$ in **2**, where the overall charge of the dimer is expressed in parentheses. The two one-electron oxidations are porphyrin-based and are observed in **2** at $E_{1/2}(+1/0)$ = +0.81 and $E_{1/2}(+2/+1)$ = +1.1 V vs $FcCp^*_2$. Here the overall charge of the porphyrin is expressed in parentheses.

As the applied potential is swept negative, two single-electron reduction waves are observed for **2** at $E_{1/2}$ = −0.72 and −1.10 V vs $FcCp^*_2$. Analogous two single-electron reductions are observed for $\mathbf{2}_{sym}$ at $E_{1/2}$ = −0.69 and −1.10 V vs $FcCp^*_2$. These reductions are ruthenium metal-based, corresponding formally to $Ru_3^{III,III,II}$-pz-$Ru_3^{III,III,II}$/$Ru_3^{III,III,II}$-pz-$Ru_3^{III,II,II}$ (0/−1) and $Ru_3^{III,III,II}$-pz-$Ru_3^{III,II,II}$/$Ru_3^{III,II,II}$-pz-$Ru_3^{III,II,II}$ (−1/−2).[25,26] As the potential is swept to more negative potentials, **2** displays

dx.doi.org/10.1021/ic501889u | Inorg. Chem. 2014, 53, 11298−11306

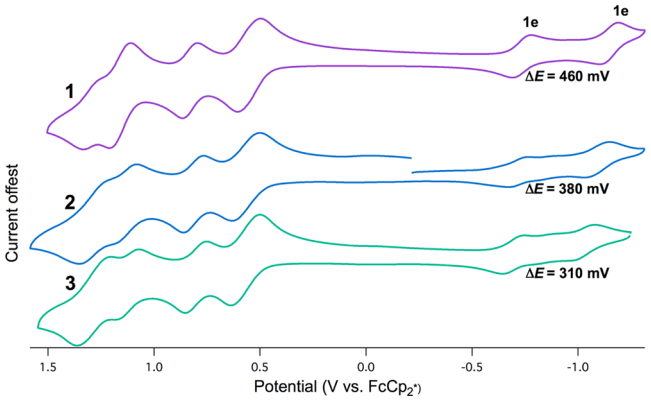

Figure 4. Cyclic voltamograms (scan rate of 100 mV/s) showing the first two reductions of **1** (top), **2** (middle), and **3** (bottom) in butyronitrile solvent and 0.1 M $TBAPF_6$ supporting electrolyte. Potentials are referenced to an external reference ($FcCp^*_2$). ΔE is the difference between the half-wave potentials for the two one-electron reduction waves corresponding to the redox processes: $Ru_3^{III,III,II}$-pz-$Ru_3^{III,III,II}$/$Ru_3^{III,III,II}$-pz-$Ru_3^{III,II,II}$ (0/−1) and $Ru_3^{III,III,II}$-pz-$Ru_3^{III,II,II}$/$Ru_3^{III,II,II}$-pz-$Ru_3^{III,II,II}$ (−1/−2).

two quasi-reversible single-electron reductions, which correspond to reductive features observed in ZnTPPpy. These porphyrin reductions agree with the literature and correspond to ZnTPPpy (0/−1) and (−1/−2).[48] The shift to more positive potentials for the second reduction feature is consistent with the coordinated ZnTPPpy donating electron density onto the Ru_3O dimer.

Figure 3 demonstrates the minimal interaction between the two redox-active domains: the ruthenium metal clusters and zinc porphyrin. Further analysis of the electrochemical reduction features for **1**−**3** allows for estimation of their stability arising from electron delocalization in the mixed-valence state through the comproportionation constant. K_c can be interpreted further in terms of the electronic coupling, H_{AB}, and the thermodynamics of electron transfer between the discrete ZnTPPpy and Ru_3O-pz-Ru_3O redox centers to be discussed.

The first two reductions across the dyad series **1**−**3** (Figure 4) show variation in both the onset potential of the first reduction process and splitting observed between the first and second reductions as a result of variation in electronic coupling. This is observed directly in the magnitude of the splitting between the single-electron (0/−1) and (−1/−2) reduction waves, ΔE, which corresponds to the stabilization energy imparted to the −1 state by electron delocalization across the dimer.[49,50] In the case of **1**, ΔE = 460 mV and $K_c = \exp(\Delta EF/RT) = 6.0 \times 10^7$ for the equilibrium given in eq 1. It is useful to consider K_c as a stability constant reflecting the stabilization arising from electronic delocalization in the −1 state relative to the neutral and −2 states.

$$Ru_3^{III,III,II}\text{-pz-}Ru_3^{III,III,II} + Ru_3^{III,II,II}\text{-pz-}Ru_3^{III,II,II} \rightleftharpoons 2Ru_3^{III,III,II}\text{-pz-}Ru_3^{III,II,II} \quad (1)$$

A noteworthy aspect of these complexes is that the splitting between (0/−1) and (−1/−2) states of **1**−**3** depends strongly on the ancillary ligand. As the pyridyl ligand is changed from an electron-donating dmap (**1**) to an unsubstitued pyridine (**2**) to the electron-withdrawing cpy (**3**), K_c decreases by more than a 2 orders of magnitude (Table 1). To the extent that ΔE values

Table 1. Electrochemical Data for $[Ru_3(\mu_3\text{-}O)(\mu\text{-}CH_3CO_2)_6(CO)(ZnTPPpy)](\mu\text{-pz})[Ru_3(\mu_3\text{-}O)(\mu\text{-}CH_3CO_2)_6(CO)(L)]$ (1−3)[a]

	L	$E_{1/2}(0/-1)$	$E_{1/2}(-1/-2)$	ΔE (mV)	K_c
1	dmap	−0.74	−1.2	460	6.0×10^7
2	py	−0.72	−1.1	380	2.7×10^6
3	cpy	−0.69	−1.0	310	1.8×10^5

[a]Cyclic voltammograms were recorded in 0.1 M $TBAPF_6$ in butyronitrile. Potentials are referenced versus $FcCp^*_2$.

reflect the magnitude of the electronic coupling, H_{AB}, it is clear that H_{AB} can be moderated over a large range by relatively simple ligand substitution, a concept explored previously in the literature.[49,50] This range of ΔE and its correlation to H_{AB} have been previously described for the symmetric dimers, and the trends are consistent with that for dyads **1**−**3**.[25,26] Previously these trends have been explained by two lines of reasoning: (i) very favorable overlap between the Ru_3O cluster dπ-electron system and the bridging pz and (ii) the ability to raise or lower Ru_3O cluster d-electron levels engaging the pz π^* system by changing the electron donor/acceptor nature of the ancillary pyridyl ligand. The relevant Ru d level then is closer in energy to the pz π^* level in **1** than it is in **3**.[26] This description is based on studies of solvent dependence of carbonyl coalescence, characterization of the intervalence charge transfer, and resonance Raman experiments.[28,29,32−34] These orbital descriptions apply well to **1**−**3**, showing a stabilizing trend in the mixed-valence species, as determined by ΔE ($\propto \ln K_c$), where $\mathbf{3}^- < \mathbf{2}^- < \mathbf{1}^-$.

Intervalence Charge Transfer. When the mixed-valence species $\mathbf{2}^-$ is prepared by chemical reduction, intervalence charge-transfer (IVCT) bands appear in the electronic absorption spectra (Figure 5). The neutral species exhibits no absorbance in the NIR region. Upon reduction to the −1 state, two broad bands appear at λ > 800 nm. These IVCT transitions have been previously described in the symmetric pyridyl dimers under the BCS semiclassical three-state model, which includes both Ru_3O redox center states and a state for the bridging

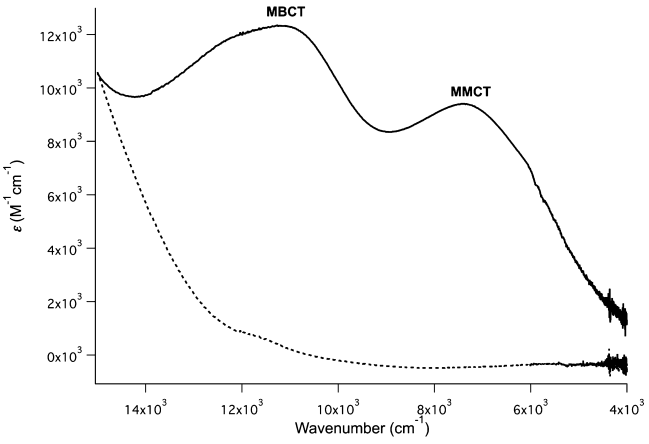

Figure 5. NIR spectra for **2** in the neutral (n = 0, dashed) and one-electron reduced (n = −1, solid) states in butyronitrile. $\mathbf{2}^-$ was generated by the stoichiometric addition of KC_8, a chemical reducing agent. The two peaks visible in the singly reduced state are identified as metal-to-metal (low energy) and metal-to-bridge (high energy) in accordance with the BCS semiclassical three-state model of mixed valency.

dx.doi.org/10.1021/ic501889u | Inorg. Chem. 2014, 53, 11298−11306

ligand.[35,51] Applying the BCS model to electronically coupled donor−bridge−acceptor assemblies results in three adiabatic potential energy surfaces: ground and excited-state surfaces involving the two metal (Ru_3O) units and an excited state involving the bridge. When the bridging ligand state is higher in energy than the two metal-based states, the low-energy transition is metal-to-metal charge-transfer (MMCT) in character and the high-energy transition is assigned to metal-bridging ligand charge-transfer (MBCT). Previous studies on the symmetric dimers have led to the conclusion that the bridging ligand π^* energy level is higher than the d-orbitals involved in the singly reduced state, thus the lowest-energy IVCT band of $\mathbf{1}^-$−$\mathbf{3}^-$ (Figure 6), observed at ca. 7300−8200

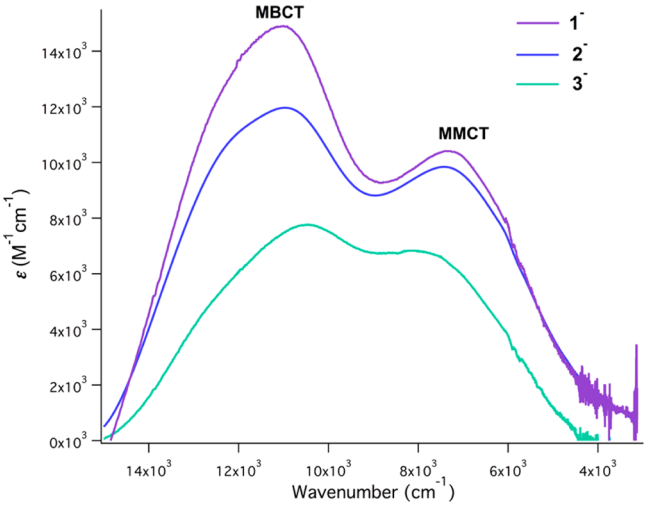

Figure 6. Difference spectra of the NIR absorbance for singly reduced $\mathbf{1}^-$−$\mathbf{3}^-$ in butyronitrile. Single-electron reduction was achieved by the stoichiometric addition of KC_8, a chemical reducing agent. To more easily fit the bands and remove absorbance of the porphyrin Q-bands, the neutral spectra was subtracted from the minus-one spectra (same concentration). The intensity of the IVCT transitions correlate to the electronic communication across the molecule in the mixed-valence state.

cm^{-1}, is assigned to MMCT, and the higher-energy band at 10 000−11 000 cm^{-1} is assigned to MBCT. Spectral deconvolution allowed each band to be fit by one Gaussian in order to extract energies for the observed metal-based electronic transitions.[52,35] The energies ($\tilde{\nu}_{max}/cm^{-1}$), molar absorptivity ($\varepsilon_{max}/M^{-1}cm^{-1}$), and full width of the band at half-height ($\Delta\tilde{\nu}_{1/2}/cm^{-1}$) of the high- and low-energy bands in butyronitrile at 298 K for $\mathbf{1}^-$− $\mathbf{3}^-$ are given in Table 2. These values are well-correlated to the peak energies of previously reported IVCT transitions of analogous systems (Table S1, Supporting Information).

Within the three-state model both MMCT and MBCT transitions increase in intensity with increasing electronic coupling in the class II regime.[35] As the electronic communication increases, the minima of the lowest three-state adiabatic potential energy surface shift toward one another (approaching a delocalized single minimum), causing the MMCT band maximum to decrease in energy and the MBCT transition to increases in energy. From $\mathbf{1}^-$ to $\mathbf{3}^-$ there is a gradual decrease in electronic communication, as the more-electron-donating ligand (dmap) increases electronic interaction between the two coupled Ru_3O units in the mixed-valence state and the electron-withdrawing ligand (cpy) decreases Ru_3O communication. Figure 6 shows the diverging MMCT and MBCT bands, as the ancillary ligand transitions from cpy to py to dmap. As predicted by the three-state model, wherein the magnitude of metal-to-bridge electronic coupling affects the lowest and highest adiabatic surfaces in opposite directions, energy shifts observed in the MBCT transition are greater than those for the MMCT transition.[35] Concomitantly, the band intensities decrease from $\mathbf{1}^-$ to $\mathbf{3}^-$ and the bands broaden significantly, reflected in the band half-width values (Table 2). The trend in stability of the mixed-valence species as determined by ΔE are consistent with the characterization of the IVCT bands resulting from a single-electron reduction; the progression from most to least delocalized mixed-valence, asymmetric porphyrin ion follows as $\mathbf{1}^- > \mathbf{2}^- > \mathbf{3}^-$.

Dynamic Carbonyl Coalescence. The vibrational spectra of **1**−**3** were obtained from chemically reduced species. Stoichiometric amounts of reducing agents KC_8 and $CoCp^*_2$ were used to prepare singly ($n = -1$) and doubly ($n = -2$) reduced states of **1**−**3**, characterized by observing the CO stretching frequency diagnostic of the electron density on each Ru_3O cluster. In the isolated ($n = 0$) state, **2** exhibits a single ν(CO) band at 1939 cm^{-1} (Figure 7). This peak displays the identical local environments and large separation of the normal modes associated with C−O stretching of the CO ligands on each $Ru_3^{III,III,II}$ cluster. The doubly reduced species also gives rise to a single ν(CO) band at 1893 cm^{-1}, reflecting identical redox states at each $Ru_3^{III,II,II}$ cluster. The ∼50 cm^{-1} shift in the ν(CO) is due to increased π-back bonding to the CO ligand, resulting from increased electron density on the cluster.[53,54] The singly reduced form of **2** displays a broad absorption band at the average of the bands observed in the isolated and doubly reduced states (ca. 1918 cm^{-1}).

Comparison of the IR spectra in the ν(CO) region of the −1 states of **1**−**3** shows the differences in spectral characteristics that arise from electronic interactions. The mixed-valence states of **1**−**3** show clear evidence of strong electronic coupling in their electrochemistry and optical spectra. The degree of coalescence of the IR spectra depends on the degree of electronic coupling between the pyrazine-linked Ru_3O clusters (Figure 7). As electronic coupling decreases from **1** to **3**, two

Table 2. Summary of Electronic Spectral Data for the IVCT Band of the Mixed-Valence (−1) State of 1−3 in Butyronitrile[a]

		MMCT			MBCT		
	L	ν_{max} (cm^{-1})	ε_{max} ($M^{-1}cm^{-1}$)	$\Delta\nu_{1/2}$ (cm^{-1})	ν_{max} (cm^{-1})	ε_{max} (M^{-1} cm^{-1})	$\Delta\nu_{1/2}$ (cm^{-1})
1	dmap	7080	9550	3600	11500	14800	4020
2	py	7100	8980	3680	11400	11800	4220
3	cpy	7120	4580	2980	10700	7530	4770

[a]Spectral deconvolution of the NIR spectra of $\mathbf{1}^-$−$\mathbf{3}^-$ was carried out using IGOR Pro's Multipeak Fit 2. In all cases, the NIR region was fit to two Gaussians.

dx.doi.org/10.1021/ic501889u | Inorg. Chem. 2014, 53, 11298−11306

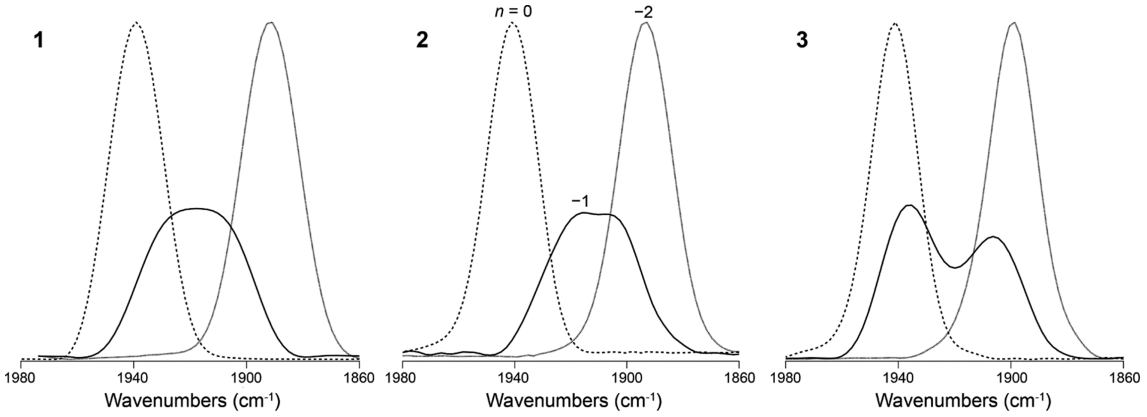

Figure 7. Infrared spectra for $\mathbf{1}^n$–$\mathbf{3}^n$ for n = 0 (- - -), −1 (—), and −2 (···) in butyronitrile. Chemical reduction was achieved with KC_8 and decamethylcobaltocene.

distinct ν(CO) bands at 1935 and 1906 cm^{-1} become resolved for **3**. Dyad **2**, with an intermediate value of electronic coupling, shows an intermediate degree of spectral coalescence in the singly reduced state. These trends are consistent with electrochemical and electronic absorption data for **1**–**3** and are also consistent with extensive studies of effects on coalescence from synthetic and environmental alterations.[34,37] The observed variation in the lineshapes representing the $Ru_3^{III,III,II}$ and $Ru_3^{III,II,II}$ states allows us to spectroscopically observe a dynamic process estimated to be occurring on a time scale shorter than 10 ps.

Photoinduced Electron-Transfer Process. Both electron and energy transfer processes can occur following porphyrin photoexcitation.[55] Although intramolecular energy transfer may occur between photoexcited ZnTPPpy* and the adjacent Ru_3O cluster [Figures S1 (Supporting Information) and 2], analysis of possible Förster energy transfer on analogous systems showed disagreement between the theoretical rates of energy transfer and experimentally measured ultrafast fluorescence quenching rates.[56] This suggests that energy transfer cannot be the exclusive mechanism responsible for the porphyrin fluorescence quenching in Ru_3O coordinated systems.

A photoinduced electron transfer would proceed as an oxidative quenching reaction to produce a porphyrin cation $ZnTPPpy^+$ and reduced $[Ru_3O\text{-pz-}Ru_3O]^-$ dimer. The free energy for electron transfer from the excited state of the Zn porphyrin to the Ru_3O-pz-Ru_3O dimer can be determined using eq 2[57]

$$\Delta G^0_{FET} = e(E^\circ_{D^{ox}/D} - E^\circ_{A/A^{red}}) - E_{00} - \frac{e^2}{4\pi\varepsilon_0\varepsilon_S R} \quad (2)$$

Here $E^\circ_{D^{ox}/D}$ and $E^\circ_{A/A^{red}}$ are the half-wave potentials for the donor oxidation and acceptor reduction, and E_{00} is the excited state energy. The stabilization energy due to Coulombic attraction in the resulting ion pair term $[e^2/(4\pi\varepsilon_0\varepsilon_S R)]$ for these experiments is approximated to be 0.1 eV (ε_0 is the permittivity in a vacuum, $\varepsilon_{butyronitrile}$ = 20.7, and R_{DA} = 6.4 Å, the center-to-center distance approximated from previously published crystallographic data).[42,58] Using the oxidation potential of ZnTPPpy (E_{ox} ca. 0.8 V vs $FcCp^*_2$ in butyronitrile), identified as the second oxidation of the dyad (Figures 3 and 4) and the potential of the first metal-based reduction (Table 1), the thermodynamic driving force for an intramolecular charge separation from the first singlet excited state of ZnTPPpy to $[Ru_3O\text{-pz-}Ru_3O]$ in **1**–**3** are presented in Table 3. In all cases, ΔG^0_{FET} is sufficiently negative, and therefore, possible intramolecular electron transfer from excited-state ZnTPPpy* to the Ru_3O-pz-Ru_3O dimer was investigated.

Table 3. Free Energy for Electron Transfer from an Excited Donor, ΔG^0_{FET}, in Butyronitrile at 25 °C[a]

	L	$E^\circ_{D^{ox}/D}$ (V)	$E^\circ_{A/A^{red}}$ (V)	E_{00} (eV)	ΔG^0_{IP} (eV)	ΔG^0_{FET} (eV)	ΔG^0_{BET} (eV)
1	dmap	0.82	−0.74	2.0	1.6	−0.54	−1.6
2	py	0.81	−0.72	2.0	1.5	−0.57	−1.5
3	cpy	0.80	−0.69	2.0	1.5	−0.62	−1.5

[a]Porphyrin donor oxidation and metal cluster acceptor reduction potential were determined electrochemically by half-wave potentials for the corresponding redox processes of **1**–**3** (Figures 3 and 4). E_{00} was determined from the average of the lowest-energy electronic transition and highest-energy emission transition (λ_{em} = 610 nm). The free energy required to generate the ion pair was determined by $-\Delta G^0_{BET}$ (eq 3).

The corresponding back electron transfer is given by eq 3:[57]

$$\Delta G^0_{BET} = e(E^\circ_{A/A^{red}} - E^\circ_{D^{ox}/D}) + \frac{e^2}{4\pi\varepsilon_0\varepsilon_S R} \quad (3)$$

The resulting free energy of back electron transfer is significantly more negative than the forward electron transfer (Table 3); therefore, in order to observe the desired singly reduced state, the back electron transfer must be inhibited. Using a sacrificial donor, the back electron transfer process following photoinduced electron transfer is predicted to be slowed through regeneration of the neutral ZnTPPpy. 1-Benzyl-1,4-dihydronicotinamide (BNAH) was chosen as a sacrificial donor for the purpose of porphyrin cation reduction following a proposed intramolecular electron transfer event. BNAH has an oxidation potential of 220 mV vs Fc/Fc^+.[59]

A solution of a 50 μM complex, 0.5 mM BNAH, and 0.1 M $TBAH_6$ in butyronitrile was prepared in a N_2 atmosphere glovebox, with care to minimize any light exposure prior to the experiment. The sample cell was sealed and an initial (pre-exposed) UV–vis/NIR spectra was collected. The cell was then exposed to 568 nm light (65 mW), with stirring, and spectra were collected at minute intervals for 50 min in total. Figure 8 shows the NIR absorption of **2** following photolysis (those of **1** and **3** can be found in Figure S4, Supporting Information). After 1.5 min of continuous photolysis, absorbance at λ > 668

dx.doi.org/10.1021/ic501889u | Inorg. Chem. 2014, 53, 11298–11306

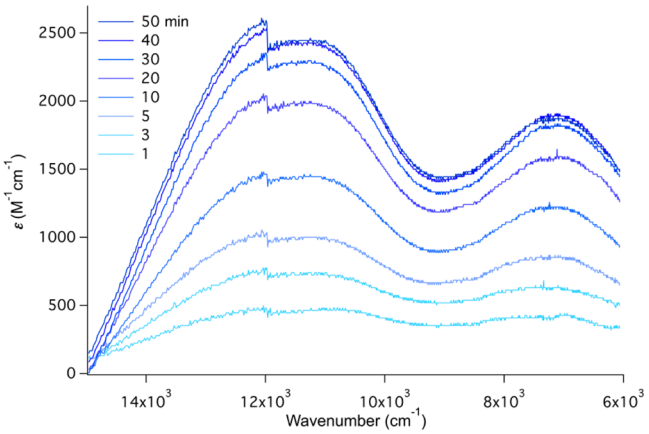

Figure 8. Difference NIR absorbance of 50 μM **2** in butyronitrile solvent with 0.1 M $TBAH_6$ and 0.50 mM sacrificial donor (BNAH) following photolysis with 568 nm light.

nm (>14 970 cm^{-1}) becomes nonzero (ε = 480 M^{-1} cm^{-1}). During the course of the experiment, this absorbance evolves into two well-defined peaks (ν_{max}/cm^{-1} = 7270 and 11300).

The observation of two IVCT bands in the NIR confirms the generation of the singly reduced mixed-valence dimer following photoexcitation of the coordinated zinc porphyrin. These IVCT transitions are identified as MBCT (high energy) and MMCT (low energy), and their peak location and intensities reflect the strong electronic coupling resulting from electron delocalization across the dimer. The observation of a strongly coupled mixed-valence state following a photoinduced intramolecular electron transfer event serves as a proof-of-concept for future measurements of the delocalization dynamics of electron transfer reactions following photodriven reductive processes.

CONCLUSION

The mixed-valence assemblies made up of two oxo-centered, triruthenium clusters and one zinc(II) 5-(4-pyridyl)-10,15,20-triphenylporphyrin ancillary ligand reported here provide new systems capable of undergoing light-induced, intramolecular electron transfer. By altering the ancillary ligand opposite the porphyrin (L = dmap, py, or cpy), the electronic environment across the entire mixed-valence inorganic system can be tuned. The effect of this tuning has been characterized electrochemically by two sequential single-electron reductions and chemically by carbonyl coalescence observed in the infrared vibrational spectrum. Two IVCT bands in the NIR diverge in energy as the ground-state potential energy surface adjusts to shift the metal-to-bridge transition to higher energy and the metal-to-metal transition to lower energy for the most electronically coupled ion $\mathbf{1}^-$. The high-energy singlet excited state of the porphyrin provides sufficient energetics for electron injection onto the pyrazine-bridged dimer, and intramolecular electron transfer was demonstrated with continuous photolysis in the presence of a sacrificial donor. The ground-state characterization of these stable, singly reduced species resulting from photoexcitation into the mixed-valence state and their corresponding strong electronic coupling encourage further studies on the time-dependent dynamics of delocalization.

ASSOCIATED CONTENT

Supporting Information

Fluorescence emission spectra of ZnTPPpy and **ii**, NIR spectra of $\mathbf{1}^n$–$\mathbf{3}^n$ in their n = 0, −1, and −2 oxidation states, MMCT/MBCT energies of symmetric pyrazine-bridged dimers, curve fits for spectra in Figure 6, and photolysis results for **1** and **3**. This material is available free of charge via the Internet at http://pubs.acs.org.

AUTHOR INFORMATION

Corresponding Author

*E-mail: ckubiak@ucsd.edu.

Notes

The authors declare no competing financial interest.

ACKNOWLEDGMENTS

The authors thank Jonas Petersson for his valuable collaboration. We also thank Prof. Michael Tauber for use of their Ag^+/Kr^+ laser and Dr. Brian Leigh for his continual enthusiasm. This work was supported by the National Science Foundation under Grant CHE-1145893.

REFERENCES

(1) Meyer, T. J. *Acc. Chem. Res.* **1989**, *22*, 163.
(2) Alstrum-Acevedo, J. H.; Brennaman, M. K.; Meyer, T. J. *Inorg. Chem.* **2005**, *44*, 6802.
(3) Gould, S. L.; Kodis, G.; Palacios, R. E.; de la Garza, L.; Brune, A.; Gust, D.; Moore, T. A.; Moore, A. L. *J. Phys. Chem. B* **2004**, *108*, 10566.
(4) Harriman, A.; Sauvage, J.-P. *Chem. Soc. Rev.* **1996**, *25*, 41.
(5) Göransson, E.; Boixel, J.; Monnereau, C.; Blart, E.; Pellegrin, Y.; Becker, H.-C.; Hammarström, L.; Odobel, F. *Inorg. Chem.* **2010**, *49*, 9823.
(6) Wasielewski, M. R. *Chem. Rev.* **1992**, *92*, 435.
(7) Albinsson, B.; Eng, M. P.; Pettersson, K.; Winters, M. U. *Phys. Chem. Chem. Phys.* **2007**, *9*, 5847.
(8) Imahori, H. *Org. Biomol. Chem.* **2004**, *2*, 1425.
(9) Abrahamsson, M.; Jäger, M.; Kumar, R. J.; Österman, T.; Persson, P.; Becker, H.-C.; Johansson, O.; Hammarström, L. *J. Am. Chem. Soc.* **2008**, *130*, 15533.
(10) Meylemans, H. A.; Lei, C.-F.; Damrauer, N. H. *Inorg. Chem.* **2008**, *47*, 4060.
(11) Sauvage, J. P.; Collin, J. P.; Chambron, J. C.; Guillerez, S.; Coudret, C.; Balzani, V.; Barigelletti, F.; De Cola, L.; Flamigni, L. *Chem. Rev.* **1994**, *94*, 993.
(12) Gust, D.; Moore, T. A.; Moore, A. L. *Acc. Chem. Res.* **1993**, *26*, 198.
(13) Harriman, A.; Odobel, F.; Sauvage, J.-P. *J. Am. Chem. Soc.* **1995**, *117*, 9461.
(14) Kavarnos, G. J.; Turro, N. J. *Chem. Rev.* **1986**, *86*, 401.
(15) Browne, W. R.; O'Boyle, N. M.; McGarvey, J. J.; Vos, J. G. *Chem. Soc. Rev.* **2005**, *34*, 641.
(16) Balzani, V.; Juris, A.; Venturi, M.; Campagna, S.; Serroni, S. *Chem. Rev.* **1996**, *96*, 759.
(17) Wenger, O. S. *Coord. Chem. Rev.* **2009**, *253*, 1439.
(18) Paddon-Row, M. N. *Acc. Chem. Res.* **1994**, *27*, 18.
(19) Miller, J. R.; Calcaterra, L. T.; Closs, G. L. *J. Am. Chem. Soc.* **1984**, *106*, 3047.
(20) Luo, C.; Guldi, D. M.; Imahori, H.; Tamaki, K.; Sakata, Y. *J. Am. Chem. Soc.* **2000**, *122*, 6535.
(21) Helms, A.; Heiler, D.; McLendon, G. *J. Am. Chem. Soc.* **1991**, *113*, 4325.
(22) Sutin, N. *Acc. Chem. Res.* **1982**, *15*, 275.
(23) Collin, J.-P.; Harriman, A.; Heitz, V.; Odobel, F.; Sauvage, J.-P. *J. Am. Chem. Soc.* **1994**, *116*, 5679.

(24) Wasielewski, M. R.; Gaines, G. L.; Wiederrecht, G. P.; Svec, W. A.; Niemczyk, M. P. *J. Am. Chem. Soc.* **1993**, *115*, 10442.
(25) Ito, T.; Hamaguchi, T.; Nagino, H.; Yamaguchi, T.; Washington, J.; Kubiak, C. P. *Science* **1997**, *277*, 660.
(26) Ito, T.; Hamaguchi, T.; Nagino, H.; Yamaguchi, T.; Kido, H.; Zavarine, I. S.; Richmond, T.; Washington, J.; Kubiak, C. P. *J. Am. Chem. Soc.* **1999**, *121*, 4625.
(27) Londergan, C. H.; Kubiak, C. P. *J. Phys. Chem. A* **2003**, *107*, 9301.
(28) Londergan, C. H.; Rocha, R. C.; Brown, M. G.; Shreve, A. P.; Kubiak, C. P. *J. Am. Chem. Soc.* **2003**, *125*, 13912.
(29) Glover, S. D.; Kubiak, C. P. *J. Am. Chem. Soc.* **2011**, *133*, 8721.
(30) Kubiak, C. P. *Inorg. Chem.* **2013**, *52*, 5663.
(31) Kido, H.; Nagino, H.; Ito, T. *Chem. Lett.* **1996**, *25*, 745.
(32) Salsman, J. C.; Kubiak, C. P.; Ito, T. *J. Am. Chem. Soc.* **2005**, *127*, 2382.
(33) Salsman, J. C.; Ronco, S.; Londergan, C. H.; Kubiak, C. P. *Inorg. Chem.* **2006**, *45*, 547.
(34) Lear, B. J.; Glover, S. D.; Salsman, J. C.; Londergan, C. H.; Kubiak, C. P. *J. Am. Chem. Soc.* **2007**, *129*, 12772.
(35) Brunschwig, B. S.; Creutz, C.; Sutin, N. *Chem. Soc. Rev.* **2002**, *31*, 168.
(36) Robin, M. B.; Day, P. In *Advances in Inorganic Chemistry and Radiochemistry*; Emeléus, H. J., Sharpe, A. G., Eds.; Academic Press: New York, 1968; Vol. *10*, p 247.
(37) Glover, S. D.; Lear, B. J.; Salsman, C.; Londergan, C. H.; Kubiak, C. P. *Philos. Trans. R. Soc. A* **2008**, *366*, 177.
(38) McCusker, J. K. *Acc. Chem. Res.* **2003**, *36*, 876.
(39) Reid, P. J.; Silva, C.; Barbara, P. F.; Karki, L.; Hupp, J. T. *J. Phys. Chem.* **1995**, *99*, 2609.
(40) Walker, G. C.; Barbara, P. F.; Doorn, S. K.; Dong, Y.; Hupp, J. T. *J. Phys. Chem.* **1991**, *95*, 5712.
(41) Lindsey, J. S.; Schreiman, I. C.; Hsu, H. C.; Kearney, P. C.; Marguerettaz, A. M. *J. Org. Chem.* **1987**, *52*, 827.
(42) Fleischer, E. B.; Shachter, A. M. *Inorg. Chem.* **1991**, *30*, 3763.
(43) Schwindt, M. A.; Lejon, T.; Hegedus, L. S. *Organometallics* **1990**, *9*, 2814.
(44) Aranzaes, J. R.; Daniel, M.-C.; Astruc, D. *Can. J. Chem.* **2006**, *84*, 288.
(45) Adler, A. D.; Longo, F. R.; Kampas, F.; Kim, J. *J. Inorg. Nucl. Chem.* **1970**, *32*, 2443.
(46) Barton, M. T.; Rowley, N. M.; Ashton, P. R.; Jones, C. J.; Spencer, N.; Tolley, M. S.; Yellowlees, L. J. *J. Chem. Soc., Dalton Trans.* **2000**, 3170.
(47) Campagna, S.; Denti, G.; Serroni, S.; Ciano, M.; Juris, A.; Balzani, V. *Inorg. Chem.* **1992**, *31*, 2982.
(48) Kadish, K.; Van Caemelbecke, E. *J. Solid State Electrochem.* **2003**, *7*, 254.
(49) Richardson, D. E.; Taube, H. *Inorg. Chem.* **1981**, *20*, 1278.
(50) Richardson, D. E.; Taube, H. *Coord. Chem. Rev.* **1984**, *60*, 107.
(51) Glover, S. D.; Goeltz, J. C.; Lear, B. J.; Kubiak, C. P. *Coord. Chem. Rev.* **2010**, *254*, 331.
(52) Hush, N. S. *Prog. Inorg. Chem.* **1967**, *8*, 391.
(53) Londergan, C. H.; Kubiak, C. P. *Chem.—Eur. J.* **2003**, *9*, 5962.
(54) Crabtree, R. H. *The Organometallic Chemistry of the Transtion Metals*, 5th ed.; Wiley: New Haven, CT, 2009.
(55) Knight, T. E.; Guo, D.; Claude, J. P.; McCusker, J. K. *Inorg. Chem.* **2008**, *47*, 7249.
(56) Wall, J. M. H.; Akimoto, S.; Yamazaki, T.; Ohta, N.; Yamazaki, I.; Sakuma, T.; Kido, H. *Bull. Chem. Soc. Jpn.* **1999**, *72*, 1475.
(57) Rehm, D.; Weller, A. *Isr. J. Chem.* **1970**, *8*, 259.
(58) Yamaguchi, T.; Imai, N.; Ito, T.; Kubiak, C. P. *Bull. Chem. Soc. Jpn.* **2000**, *73*, 1205.
(59) Fukuzumi, S.; Hironaka, K.; Nishizawa, N.; Tanaka, T. *Bull. Chem. Soc. Jpn.* **1983**, *56*, 2220.